Molecular Biology of the Cell
Vol. 19, 3871–3884, September 2008

Coordinated Lipid Transfer between the Endoplasmic Reticulum and the Golgi Complex Requires the VAP Proteins and Is Essential for Golgi-mediated Transport

Diego Peretti,* Nili Dahan,* Eyal Shimoni,† Koret Hirschberg,‡ and Sima Lev*

*The Molecular Cell Biology Department and the †Electron Microscopy Unit, Weizmann Institute of Science, Rehovot 76100, Israel; and ‡Department of Pathology, Faculty of Medicine, Tel-Aviv University, Ramat Aviv 69978, Israel

Submitted May 19, 2008; Revised June 16, 2008; Accepted June 23, 2008
Monitoring Editor: Vivek Malhotra

Lipid transport between intracellular organelles is mediated by vesicular and nonvesicular transport mechanisms and is critical for maintaining the identities of different cellular membranes. Nonvesicular lipid transport between the endoplasmic reticulum (ER) and the Golgi complex has been proposed to affect the lipid composition of the Golgi membranes. Here, we show that the integral ER–membrane proteins VAP-A and VAP-B affect the structural and functional integrity of the Golgi complex. Depletion of VAPs by RNA interference reduces the levels of phosphatidylinositol-4-phosphate (PI4P), diacylglycerol, and sphingomyelin in the Golgi membranes, and it leads to substantial inhibition of Golgi-mediated transport events. These effects are coordinately mediated by the lipid-transfer/binding proteins Nir2, oxysterol-binding protein (OSBP), and ceramide-transfer protein (CERT), which interact with VAPs via their FFAT motif. The effect of VAPs on PI4P levels is mediated by the phosphatidylinositol/phosphatidylcholine transfer protein Nir2, which is required for Golgi targeting of OSBP and CERT and the subsequent production of diacylglycerol and sphingomyelin. We propose that Nir2, OSBP, and CERT function coordinately at the ER–Golgi membrane contact sites, thereby affecting the lipid composition of the Golgi membranes and consequently their structural and functional identities.

INTRODUCTION

The unique lipid compositions of the secretory and endocytic organelles are critical for maintaining their distinct structural and functional identities (van Meer, 2000). Their identities are maintained despite extensive interconnecting vesicular-trafficking pathways, and they require tight regulation of lipid sorting, metabolism, and transport (van Meer, 1993; Pomorski *et al*., 2001; van Meer and Sprong, 2004). Increasing lines of evidence suggest that lipid-transfer proteins (LTPs) play a major role in regulating the lipid composition of membranous organelles (Sprong *et al*., 2001; De Matteis *et al*., 2007). These proteins facilitate lipid transfer between a donor and acceptor membrane (Holthuis and Levine, 2005), and they usually contain dual-targeting determinants for different membrane compartments. LTPs have been proposed to efficiently transfer lipids at membrane contact sites (MCSs) (Holthuis and Levine, 2005; Levine and Loewen, 2006).

MCSs or zones of close apposition between the ER membranes and other cellular membranes, including the plasma membrane (PM), the membranes of the vacuoles, mitochondria, peroxisomes, lipid droplets, late endosomes, lysosomes, and the Golgi apparatus, have been identified in all eukaryotes by morphological and biochemical studies (Shore and Tata, 1977; Levine, 2004; Levine and Loewen, 2006). More recently, electron tomography studies have identified close contacts (10–20 nm) between the ER and the outer mitochondrial membrane (Perkins *et al*., 1997) and between a specialized *trans*-ER and the three *trans*-most cisternae of the Golgi complex (Ladinsky *et al*., 1999; Marsh *et al*., 2001, 2004). This specialized *trans*-ER, which is continuous with the entire ER network, was proposed to be involved in modifying the lipid composition of the *trans*-cisternal Golgi membranes by permitting direct transfer of lipids, such as ceramide, between ER and Golgi membranes (Ladinsky *et al*., 1999; Mogelsvang *et al*., 2004). Consistent with this hypothesis, reconstitution studies using a cell-free system provided biochemical evidence that ER–Golgi membrane contacts are required for nonvesicular ceramide transport (Funato and Riezman, 2001), and more recently, that the ceramide-transfer protein, CERT, efficiently transfers ceramide from the ER to the Golgi at the ER–Golgi MCSs (Hanada *et al*., 2003; Kawano *et al*., 2006).

This article was published online ahead of print in *MBC in Press* (http://www.molbiolcell.org/cgi/doi/10.1091/mbc.E08–05–0498) on July 9, 2008.

Address correspondence to: Sima Lev (sima.lev@weizmann.ac.il).

Abbreviations used: 25OH, 25-hydroxycholesterol; AP1, adaptor complex 1; CERT, ceramide-transport protein; GFP-PKCη-C1b, C1b domain of PKCη fused to GFP; CCT, CTP:phosphocholine cytidylyltransferase; DAG, diacylglycerol; ER, endoplasmic reticulum; FFAT, two phenylalanines in an acidic tract; KDEL-R, KDEL receptor; LT/BP, lipid-transfer/binding protein; MCS, membrane contact site; ET-18-OCH_3, *O*-octadecyl-2-*O*-methyl-*rac*-glycero-3-phosphocholine; OSBP, oxysterol-binding protein; PC, phosphatidylcholine; PH, pleckstrin homology; PI, phosphatidylinositol; PI4K, phosphatidylinositol 4-kinase; PI4P, phosphatidylinositol-4-phosphate; GFP-PKD, protein kinase D; RNAi, RNA interference; siRNA, small interfering RNA; SM, sphingomyelin; TGN, *trans*-Golgi network; VAP, vesicle-associated membrane protein-associated proteins.

CERT contains dual-targeting determinants for the ER and the Golgi membranes. It interacts with the Golgi through its pleckstrin homology (PH) domain that binds phosphatidylinositol-4-phosphate (PI4P), and with the ER membranes through its FFAT (two phenylalanines in an acidic tract) motif that interacts with the integral ER–membrane proteins of the vesicle-associated membrane protein-associated protein (VAP) family: VAP-A and VAP-B (VAPs) (Hanada, 2006).

VAPs are type II integral membrane proteins, sharing 63% amino acid identity and similar basic primary organization. They are composed of an N-terminal immunoglobulin-like β sheet that shares homology with the well-characterized major sperm protein (MSP), a central coiled-coil domain, and a C-terminal transmembrane domain (Lev *et al.*, 2008). VAPs recruit FFAT-motif–containing proteins to the cytosolic surface of the ER membranes, through a conserved region within their MSP domain (Kaiser *et al.*, 2005), and they have been implicated in regulation of membrane transport, phospholipid biosynthesis, and the unfolded protein response. Although their role in maintaining the identities of intracellular organelles has not been demonstrated, their ability to interact with lipid-transfer/binding proteins (LT/BPs) (Loewen *et al.*, 2003) may affect the lipid composition of certain cellular membranes.

Previous studies have shown that VAPs interact with the FFAT-motif–containing proteins Nir2 (Amarilio *et al.*, 2005), oxysterol-binding protein (OSBP) (Wyles *et al.*, 2002), and CERT (Kawano *et al.*, 2006). These three LT/BPs, which shuttle between the cytosol and the Golgi complex, are potentially functionally interdependent: CERT transports ceramide from the ER to the Golgi, and ceramide and PC are converted into sphingomyelin (SM) and diacylglycerol (DAG) by SM synthase (SMS) in the *trans*-Golgi (Hanada *et al.*, 2007). Nir2 is a phosphatidylinositol/phosphatidylcholine (PI/PC)-transfer protein that is involved in the regulation of DAG levels at the Golgi apparatus through inhibition of the CDP-choline pathway for PC biosynthesis (Litvak *et al.*, 2005). Overexpression of OSBP enhances SM production in the presence of its high-affinity ligand, 25-hydroxycholesterol (25OH) (Lagace *et al.*, 1999), and current studies suggest that OSBP is required for sterol-dependent activation of CERT (Perry and Ridgway, 2006). Thus, it could be that these VAP-binding proteins are coordinately involved in regulating the lipid composition of the ER and/or Golgi membranes, thereby affecting the structural and functional properties of these organelles.

In this study, we show that VAPs play a critical role in maintaining the structural and functional properties of the Golgi complex. We found that knockdown of VAP reduces the levels of PI4P, DAG, and SM in the Golgi membranes and exerts pleiotropic effects on Golgi-mediated transport. We provide evidence that the effects of VAPs are mediated by their interacting FFAT-motif–containing proteins Nir2, OSBP, and CERT, and we further demonstrate the coordinated functions of these LT/BPs. Accordingly, we propose that VAPs provide a scaffold for these LT/BPs at the ER–Golgi MCSs, thereby affecting the lipid composition of the Golgi membranes and consequently their structural and functional identities.

MATERIALS AND METHODS

Constructs, Antibodies, and Chemicals

Mammalian expression vectors encoding the green fluorescent protein (GFP)-PKD, GFP-PH-OSBP, GFP-PKCη-C1b, GFP-*N*-acetylglucosaminyl-transferase I (NAGT-I), GFP-VAP-A, and GFP-CERT fusion proteins were kindly provided by C. Brodie (Bar-Ilan University, Ramat-Gan, Israel), S. Munro (MRC Laboratory of Molecular Biology, Cambridge, United Kingdom), E. Livneh (Ben Gurion University, Beersheba, Israel), D. Shima (Imperial Cancer Research Fund, London, United Kingdom), and P. A. Skehel (University of Edinburgh, Edinburgh, United Kingdom), and K. Hanada (National Institute of Infectious Diseases, Tokyo, Japan), respectively. DNA constructs encoding either the wild-type Nir2-HA and its mutants, and the PI-transfer domain (amino acids [aa] 1-277), or the VAP-B-Myc, as well as antibodies against Nir2 and VAP were described previously (Amarilio *et al.*, 2005; Litvak *et al.*, 2005). Polyclonal antibodies against GRASP65 were raised in rabbits against glutathione-S-transferase fusion protein consisting amino acids 240-440 of the human GRASP65. Monoclonal anti-hemagglutinin (HA), anti-Myc and anti-KDEL receptor (KDEL-R) antibodies, as well as polyclonal anti-protein disulfide isomerase (PDI) antibody were purchased from Santa Cruz Biotechnology (Santa Cruz, CA). Monoclonal antibodies against β-COP, Calnexin, and γ-adaptin were purchased from Sigma-Aldrich (St. Louis, MO). Polyclonal antibody against TGN46 was from Serotec (Oxford, United Kingdom), and polyclonal antibody to Cathepsin D was from Calbiochem (EMD Biosciences, La Jolla, CA). Monoclonal anti-vesicular stomatitis virus G (VSV-G) and polyclonal anti-GS28 antibodies were kindly provided by Z. Elazar (Weizmann Institute of Science, Rehovot, Israel). Monoclonal anti-p115 and -CERT antibodies were kindly provided by D. Shields (Albert Einstein College of Medicine, New York, NY), and J. Saus (Centro de Investigacion Principe Felipe, Valencia, Spain), respectively. Polyclonal anti-OSBP antibodies were kindly provided by M. A. De Matteis (Consorzio Mario Negri Sud, Santa Maria Imbaro, Italy) and by H. Arai (University of Tokyo, Tokyo, Japan). Alexa-488 donkey anti-mouse and anti-rabbit immunoglobulin Gs (IgGs) were purchased from Invitrogen (Carlsbad, CA). Cyanine (Cy)3-conjugated goat anti-rabbit and goat anti-mouse IgGs, as well as rhodamine donkey anti-sheep IgG, were purchased from Jackson ImmunoResearch Laboratories (West Grove, PA). 25OH and *O*-octadecyl-2-*O*-methyl-*rac*-glycero-3-phosphocholine (ET-18-OCH_3) were purchased from Sigma-Aldrich.

Cell Culture and Transfection

HeLa cells were grown in DMEM supplemented with 10% fetal bovine serum, 100 mg/ml penicillin, and 100 mg/ml streptomycin. The cells were either transfected with DNA constructs by using the calcium-phosphate method, or with small interfering RNA (siRNA) duplexes (150 nM) by using Lipofectamine 2000 (Invitrogen, Karlsruhe, Germany) according to the manufacturer's instructions. The following siRNA duplexes were used: siRNA duplex corresponding to nucleotides 449-467 of the human VAP-A cDNA (GenBank accession no. NM_003574), nucleotides 726-746 of human VAP-B cDNA (GenBank accession no. NM_004738), and nucleotides 2238-2260 of human Nir2 cDNA (GenBank accession no. AF334584). The siRNAs were synthesized by Dharmacon RNA Technologies (Lafayette, CO). Where indicated, control or RNA interference (RNAi)-treated cells were transfected with expression vectors encoding various DNA constructs 12–18 h before analysis. 25OH (2 μg/ml) was added to cells in medium containing 10% delipidated fetal bovine serum for 12 h before analysis, whereas 10 μM ET-18-OCH_3 was added for 2 h before analysis.

Immunofluorescence and Electron Microscopy

Transfected HeLa cells were grown on coverslips, washed with phosphate-buffered saline (PBS), and fixed either in methanol for 1 h at −20°C, in 1% paraformaldehyde (PFA) in KM buffer [10 mM 2-(*N*-morpholino)ethanesulfonic acid, pH 6.2, 10 mM NaCl, 1.5 mM $MgCl_2$, and 2.5% glycerol], or in 4% PFA in PBS for 20 min at room temperature, and immunostained as described previously (Litvak *et al.*, 2005). The specimens were analyzed by a confocal laser scanning microscope (Zeiss 510; Carl Zeiss, Jena, Germany) by using the 488-nm, 543-nm, and either 405- or 633-nm excitation for fluorescein, Cy3 epifluorescence and either 4,6-diamidino-2-phenylindole or Cy5, respectively. Images were processed using Adobe Photoshop (Adobe Systems, Mountain View, CA). Image data were quantified by measuring total cellular fluorescence (except nuclei) and Golgi-associated fluorescence using the colocalization function of LSM 510 software (Carl Zeiss). LysoTracker loading was performed according to the manufacturer's instructions (Invitrogen). Briefly, control and VAP-depleted HeLa cells were incubated with medium containing 75 nM LysoTracker Red DND-99 (Invitrogen) for 90 min at 37°C, washed, fixed, and analyzed by confocal microscopy. For live-cell imaging, HeLa cells transiently expressing the yellow fluorescent protein (YFP)-VSV-G (ts045) were imaged at 32°C by using a 510 confocal microscope (Carl Zeiss) equipped with a heated stage. Images were collected as described in legends. For transmission electron microscopy (TEM), control and VAP-RNAi–treated HeLa cells were grown in normal media or treated with 25OH for 12 h as indicated. The cells were fixed for 60 min in Karnovsky's fixative (3% paraformaldehyde, 2% glutaraldehyde, and 5 mM $CaCl_2$ in 0.1 M cacodylate buffer, pH 7.4, containing 0.1 M sucrose), and then washed and scraped. The cell pellet was embedded in agar noble (1.7%) and postfixed with 1% OsO_4, 0.5% potassium dichromate, and 0.5% potassium haxacyanoferrate in 0.1 M cacodylate buffer. The cells were stained en bloc with 2% aqueous uranyl acetate, followed by ethanol dehydration. Sections were cut using a diamond knife (Diatome, Biel, Switzerland) and stained by 2% uranyl acetate in water

and lead citrate. The samples were examined with transmission electron microscope Tecnai T12 (FEI, Eindhoven, Holland), at an accelerating voltage of 120 kV. Images were recorded with a 2k × 2k Eagle charge-coupled device camera (FEI, Eindhoven, Holland).

VSV-G Transport Assays

The ts045 strain of VSV was kindly provided by Z. Elazar (Weizmann Institute of Science). HeLa cells grown in 24-well plates were infected with the virus (>10 plaque-forming units/cell) in serum-free media for 45 min at 37°C. The cells were washed extensively and then incubated at 40°C for 3 h in complete media. Cycloheximide (100 μg/ml) was added 30 min before the end of the 3-h incubation period at 40°C and was present throughout the entire experiments. The cells were then shifted to 20°C for 2.5 h to accumulate VSV-G in the TGN and finally to 32°C for the indicated time periods to allow TGN export. The cells were fixed in methanol and immunostained with anti-VSV-G antibody. The rate of VSV-G export from the TGN was determined by calculating the ratio of Golgi-associated VSV-G, which was determined by colocalization with TGN46, and total VSV-G fluorescence, by using the analySIS software (Soft Imaging System, Münster, Germany). To monitor the acquisition of endoglycosidase H (endo H) resistance, control and VAPs RNAi-treated HeLa cells grown in 60-mm plates were transfected with YFP-VSV-G, and they were pulse-labeled with 200 μCi of [^{35}S]methionine (PerkinElmer Life and Analytical Sciences, Boston, MA) for 30 min at 40°C. The cells were then shifted to 32°C for the indicated times, lysed in 400 μl of lysis buffer (10 mM Tris-HCl, pH 7.4, 66 mM EDTA, 0.4% deoxycholate, 1% NP-40, and proteases inhibitors) and centrifuged at 12,000 × *g* for 1 min. The supernatant was subjected to immunoprecipitation with anti-VSV-G monoclonal antibody. After washing extensively with high-salt buffer (0.1% SDS, 0.5% (vol/vol) NP-40, 10 mM Tris-HCl, pH 7.2, 0.5 M NaCl, and 1 mM EDTA) and once with PBS, immunoprecipitated proteins were eluted from the beads into 15 μl of B1 buffer (0.1% Triton X-100, 1% SDS, and 0.1 M sodium acetate, pH 5.5) at 95°C for 5 min. The supernatant was recovered by centrifugation and was added to 45 μl of B2 buffer (0.1 M sodium acetate, pH 5.5, and protease inhibitors). Subsequently, half the sample was digested with 5 mU endo-H (Roche Diagnostics, Mannheim, Germany) for 16 h at 37°C, and the other half was taken as an undigested control. Samples were resolved by SDS-polyacrylamide gel electrophoresis (PAGE) and analyzed by autoradiography.

Cellular Fractionation

Control and VAP-depleted HeLa cells were treated with 25OH, washed in PBS, and harvested in hypotonic buffer (20 mM HEPES, pH 7.4, and 1 mM EDTA) containing protease inhibitors (1 mM phenylmethylsulfonyl fluoride, 10 μg/ml leupeptin, and 10 μg/ml aprotinin). The homogenates were incubated for 20 min on ice and sheared by passage through a 23-gauge needle. Nuclei were removed by centrifugation at 500 × *g*, and the supernatant was centrifuged at 10,000 × *g* for 15 min to isolate the heavy membrane fraction. Cytosol and light membrane fractions were obtained by centrifugation of the supernatant from the 10,000 × *g* centrifugation step for 45 min at 400,000 × *g*. Protein concentrations were determined by the Bradford assay (Bio-Rad, Hercules, CA), and an equal amount of protein was loaded onto a 12% SDS-PAGE.

Coimmunoprecipitation Studies

HeLa cells grown in 90-mm plates in the absence or presence of 2 μg/ml 25OH (for 12 h) were incubated with 2 mM dithiobis(succinimidyl propionate (Pierce Chemical, Rockford, IL), a reversible cross-linker, for 60 min at 4°C. The cells were then incubated with 20 mM Tris-HCl, pH 7.4, for 15 min at 4°C, to quench the cross-linking reaction. The cells were lysed in lysis buffer (10 mM sodium phosphate, pH 7.4, 150 mM NaCl, 5 mM KCl, 2 mM EDTA, 2 mM EGTA, 0.5% Triton X-100, and protease inhibitors) and centrifuged at 16,000 × *g* for 15 min at 4°C. VAP proteins were immunoprecipitated from the supernatants using the anti-VAPs antibody (Amarilio *et al*., 2005). The immunoprecipitates were washed three times with lysis buffer and boiled for 5 min in sample buffer containing 50 mM dithiothreitol, to cleave the cross-linker. The samples were then separated on SDS-PAGE and analyzed by Western blotting.

Cathepsin D Metabolic Labeling

Metabolic labeling of cells was carried out as described previously (Mardones *et al*., 2007), with slight modifications. Briefly, cells grown in 60-mm plates were pulse labeled for 2 h at 20°C by using 0.1 mCi/ml [^{35}S]methionine-cysteine (Perkin Elmer, Boston, MA) and chased for 1–4 h at 37°C in medium containing 5 mM mannose 6-phosphate, 0.06 mg/ml methionine, and 0.1 mg/ml cysteine. At each time point, cells were rinsed twice with PBS and lysed in buffer containing 50 mM Tris-HCl, pH 7.5, 150 mM NaCl, 10% glycerol, 5 mM EDTA, 1% (vol/vol) Triton X-100, and protease inhibitors. The extracts were immunoprecipitated using anti-Cathepsin D antibody and analyzed by SDS-PAGE and fluorography.

[^{3}H]Choline Labeling

VAPs RNAi- or scrambled siRNA-treated HeLa cells grown in 60-mm dishes (4×10^5 cells/dish) were incubated in complete medium containing 5 μCi/ml [^{3}H]methyl choline (GE Healthcare, Little Chalfont, Buckinghamshire, United Kingdom) for 12 h in the presence or absence of 2 μg/ml 25OH. The cells were then washed with PBS, harvested in 0.4 ml of cold water, and an aliquot was taken for protein determination. Lipids were extracted as described previously (Litvak *et al*., 2005), and resolved by thin layer chromatography (TLC) using chloroform:methanol:ammonia (65:35:5), as the developing solvent. Regions corresponding to PC and SM were verified by comigration with PC and SM standards, scraped from the silica plate and radioactivity was counted in a Packard (TriCarb) 1600CA liquid scintillation analyzer (PerkinElmer Life and Analytical Sciences).

RESULTS

Knockdown of VAPs Affects the Golgi Morphology

To examine whether VAPs affect the structural and functional properties of the ER and/or the Golgi complex, we down-regulated their expression in mammalian cells using the siRNA approach. Western analysis of HeLa cells expressing either a GFP-tagged VAP-A or Myc-tagged VAP-B protein demonstrated the specificity of these siRNAs for the corresponding VAP protein (Figure 1A). A mixture of these siRNAs was used to down-regulate the expression of endogenous VAPs in HeLa cells. As shown, the VAP siRNAs substantially reduced the expression of VAP-A and B within 72 h, as determined either by Western blotting (Figure 1B) or by immunofluorescence analysis (Figure 1C) using an anti-VAP antibody that recognizes both VAP proteins (Figure 1D). Immunofluorescence analysis of VAP-depleted cells using organelle-specific markers revealed that most of the intracellular organelles, including the ER (Figure 1C), lysosomes, endosomes, as well as the microtubule cytoskeleton retained their characteristic structure (Supplemental Figure S1). The Golgi apparatus, however, displayed an unusual morphology and various Golgi markers lost their compact perinuclear localization in VAP-depleted cells grown under regular growth conditions (Figure 2A). Remarkably, the effect was more pronounced in cells that were treated with 25OH for 12 h, and several Golgi markers, including the *medial*- and *trans*-Golgi proteins, NAGT-I and β1,4-galactosyltransferase I, respectively, appeared in long tubules emanating from the dispersed Golgi complex.

It has previously been shown that 25OH enhances CERT-mediated ceramide transport from the ER to the Golgi in an OSBP- and VAP-dependent manner (Perry and Ridgway, 2006). Moreover, our localization studies revealed that the VAP proteins lose their characteristic reticular distribution and are redistributed to the perinuclear region in response to 25OH (Supplemental Figure S2). These results suggest that 25OH facilitates the recruitment of VAP proteins to the ER-Golgi MCSs, and it was therefore used throughout this study.

To further characterize the effect of VAP depletion on Golgi morphology, control and VAP-depleted HeLa cells were analyzed by TEM. Control HeLa cells grown in normal media (Figure 2Ba) or those exposed to 25OH (Figure 2Bb) exhibit an obvious highly organized Golgi apparatus with a characteristic ribbon-like structure consisting of stacks of four to six flattened cisternae. In several cases, we could detect a close apposition between the ER membranes and a putative *trans*-Golgi cisterna after treatment with 25OH (Figure 2Bb, arrow). This further suggests that 25OH facilitates and/or stabilizes ER-Golgi MCSs, and is consistent with its effect on VAPs redistribution (Supplemental Figure S2). In contrast, the Golgi complex lost its characteristic organization in VAP-depleted cells treated with 25OH. The unusual morphology (Figure 2B, c–f) occurred in several typical

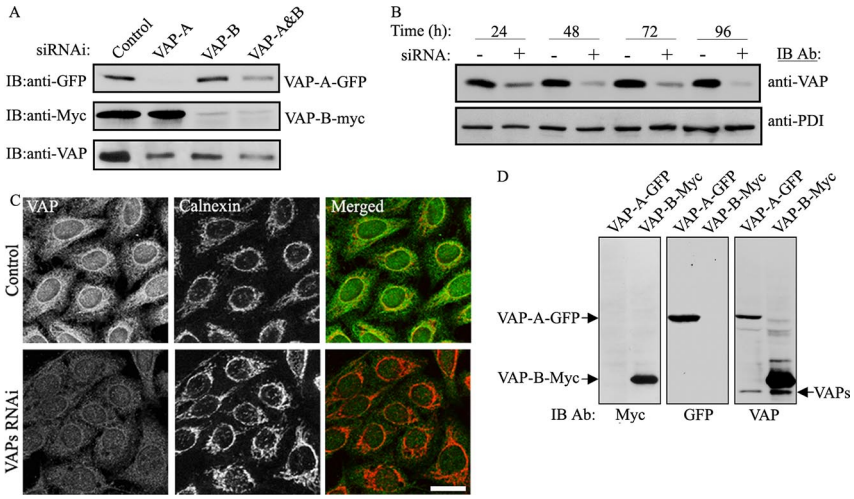

Figure 1. Down-regulation of VAPs by RNAi. (A) HeLa cells were either transfected with scrambled (control), VAP-A, VAP-B, or a mixture of VAP-A and VAP-B siRNA duplexes. Forty-eight hours later, the cells were either transfected with VAP-A-GFP, VAP-B-Myc, or left untransfected. Total cell lysate was prepared 24 h later, and the expression level of VAP-A-GFP, VAP-B-Myc, and endogenous VAPs was determined by Western blotting by using the indicated antibodies. (B) HeLa cells were transfected with a mixture of VAP-A and -B siRNA duplexes for the indicated times. The expression of VAPs was determined by immunoblotting with anti-VAP antibody, which recognizes the VAP-A and VAP-B proteins (as shown in D). The specificity of the VAPs RNAi was demonstrated by immunoblotting with anti-PDI antibody. (C) HeLa cells were either transfected with scrambled (control) or VAPs siRNA duplexes. Seventy-two hours later, the cells were fixed, coimmunostained with polyclonal anti-VAP and monoclonal anti-Calnexin antibodies, and analyzed by confocal microscopy. Bar, 10 μm. (D) Total cell lysates of HeLa cells expressing either the VAP-A-GFP or the VAP-B-Myc protein were analyzed by Western blotting using the indicated antibodies.

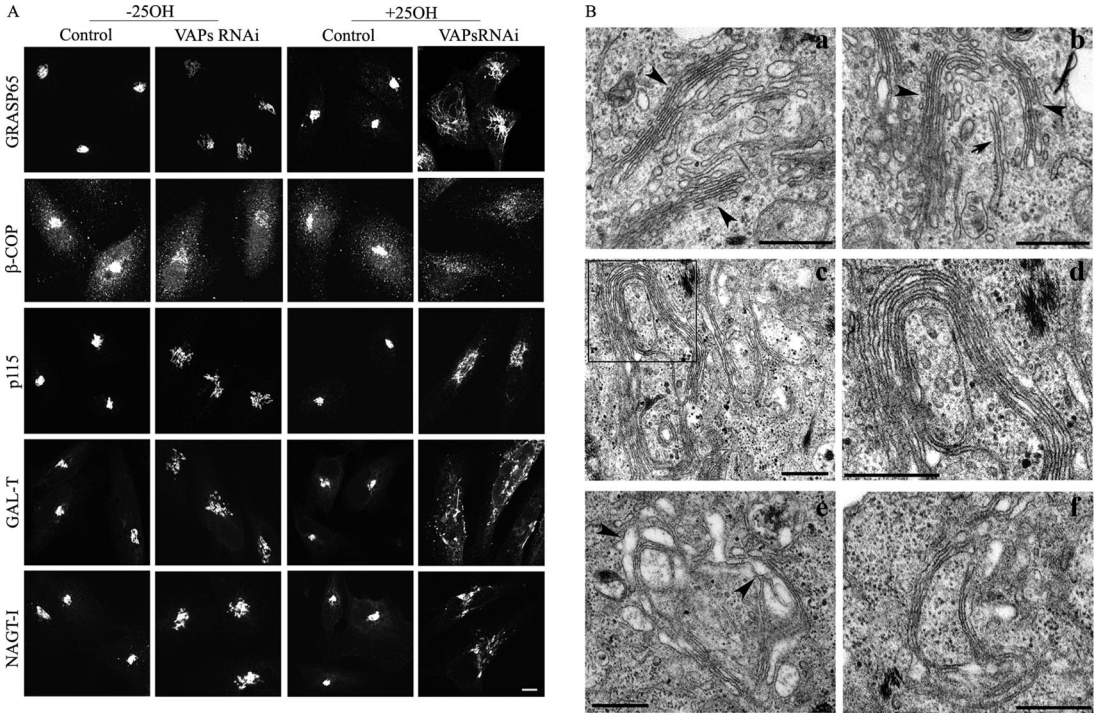

Figure 2. Knockdown of VAPs affects the Golgi structure. (A) Control and VAPs RNAi-treated cells were either grown in regular media or treated with 25OH for 12 h, fixed, and immunostained with the indicated Golgi markers. Shown are representative confocal images of VAPs RNAi and control untreated cells under the indicated growth conditions. Bar, 10 μm. (B) Control and VAPs RNAi-treated cells were either grown in regular media or treated with 25OH for 12 h, fixed as described in *Materials and Methods*, and analyzed by TEM. Representative images of control HeLa cells grown in normal media (a) or in the presence of 25OH (b), as well as 25OH-treated VAP-depleted cells (c–f) are shown. In control cells, the Golgi retains its characteristic structure consisting stacks (arrowhead) of four to six cisternae with a typical *cis-trans* morphology. Similar morphology was observed in 25OH treated cells. In some cases, proximity between a presumed *trans*-face of Golgi and the ER membrane was detected (arrow) (*b*). The Golgi lost its characteristic ribbon-like structure in 25OH-treated VAP-depleted HeLa cells (c) and elongated cisternae were detected. Larger magnification of the squared area (c) is shown in d. The disorganized Golgi structure (f) with swollen cisternae (arrowhead) is shown in e. Bar, 500 nm.

forms, including very elongated cisternae that apparently continued along several stacks to form an abnormal ribbon-like structure (Figure 2B, c and d) or a disorganized Golgi structure with swollen cisternae (Figure 2B, e and f). This unusual morphology is consistent with the immunofluorescence analysis shown in Figure 2A.

Depletion of VAPs Affects the Golgi Targeting of Nir2, OSBP, and CERT

The striking effect of VAP knockdown on the Golgi morphology led us to characterize the subcellular localization of the FFAT-motif–containing proteins Nir2, OSBP, and CERT,

using indirect immunofluorescence and confocal microscopy analysis. OSBP (Figure 3A), CERT (Figure 3B), and Nir2 (Figure 3C) were localized mainly to the Golgi complex of control cells, consistent with previous reports (Storey *et al*., 1998; Litvak *et al*., 2002), and treatment with 25OH markedly enhanced their Golgi association, as determined by

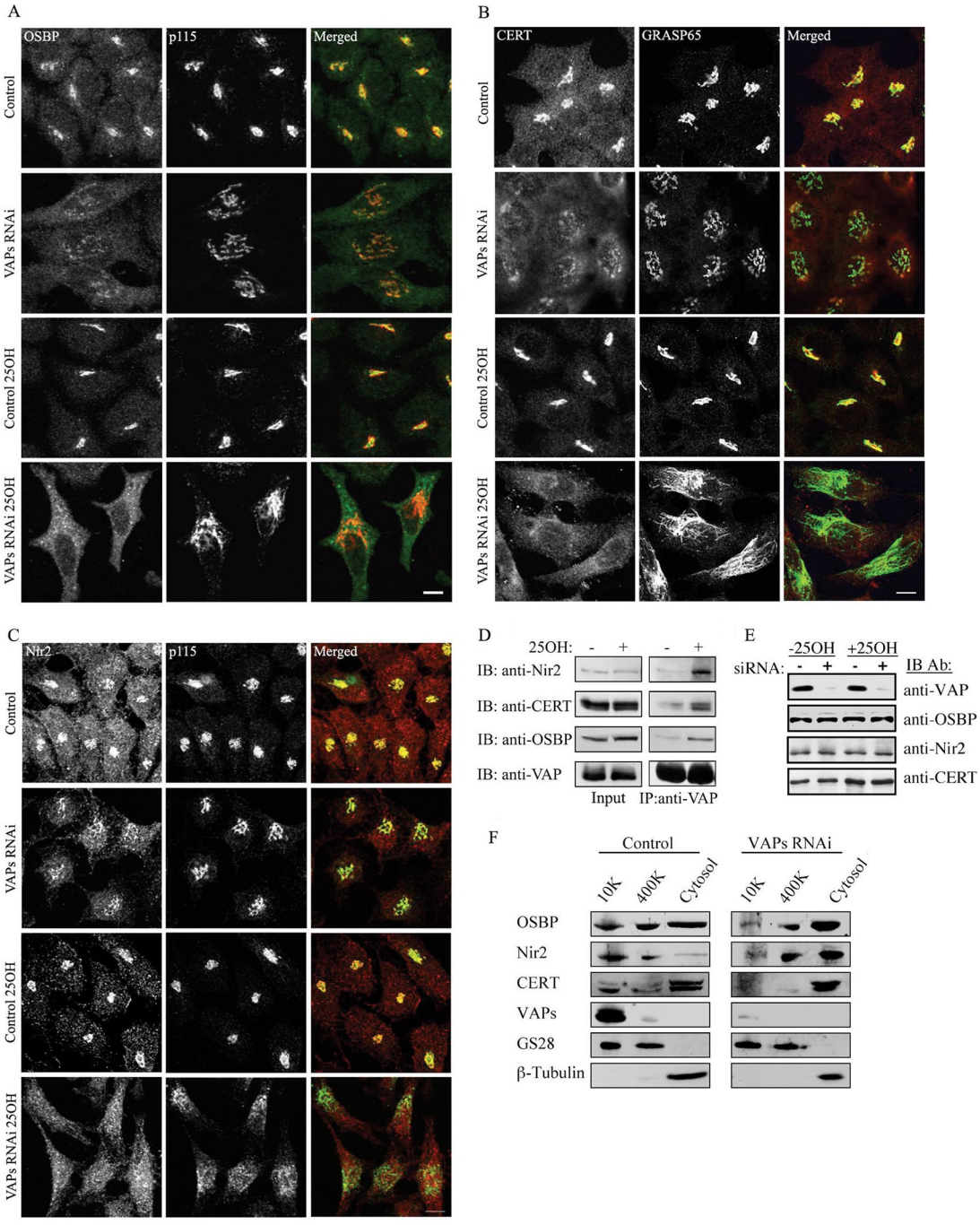

Figure 3. Knockdown of VAPs affects the Golgi-targeting of OSBP, CERT, and Nir2. Control and VAPs siRNA-transfected HeLa cells were either treated with 25OH for 12 h or left untreated. The cells were then fixed and either double-immunostained with anti-OSBP (green) and anti-p115 (red) antibodies (A), anti-CERT (red) and anti-GRASP65 (green) antibodies (B), or anti-Nir2 (red) and anti-p115 (green) antibodies (C). Bar, 10 μm. (D) The interaction between VAPs and CERT, OSBP, or Nir2 in control and 25OH-treated HeLa cells was determined by coimmunoprecipitation studies by using anti-VAP antibody for immunoprecipitation (IP) and the indicated antibody for immunoblotting (IB). (E) The expression levels of OSBP, CERT, and Nir2 in control and VAP-depleted HeLa cells were determined by Western blotting by using the corresponding antibodies. (F) Control and VAP-RNAi HeLa cells were treated with 25OH, homogenized in hypotonic buffer, and fractionated into cytosolic, light and heavy membrane (10K) fractions. An equal amount of protein (30 μg) from each fraction was separated on 12% SDS-PAGE, transferred to a nitrocellulose membrane, and immunoblotted with the indicated antibodies. The Golgi soluble *N*-ethylmaleimide-sensitive factor attachment protein receptor GS28 and β-tubulin were used as positive controls for membrane and cytosolic fractions, respectively.

colocalization with Golgi markers. This treatment also enhanced their interaction with VAPs as demonstrated by coimmunoprecipitation studies (Figure 3D). Depletion of VAPs, however, increased their cytosolic distribution under normal growth conditions, an effect that was even more pronounced in response to 25OH. Their expression levels, however, were unaffected by VAP knockdown (Figure 3E). These results suggest that the targeting of OSBP, CERT, and Nir2 to the Golgi complex in response to 25OH is dependent on the VAP proteins.

To further examine the effect of VAP knockdown on the distribution of Nir2, OSBP, and CERT, cell fractionation studies were used. As shown, the cytosolic fraction of Nir2 was markedly increased in VAP-RNAi cells treated with 25OH compared with control (Figure 3F). An increase in the cytosolic fraction of CERT and OSBP with a concomitant decrease in their membrane associated fractions was also observed in VAP-knockdown cells. However, significant levels of CERT and OSBP were also detected in the cytosolic fractions of the control cells treated with 25OH, inconsistent with their distribution seen by the immunofluorescence analysis. These results suggest that under the experimental conditions used, their membrane association was not fully maintained.

VAP-Depletion Reduces the Levels of PI4P, SM, and DAG in the Golgi Complex

Previous studies have shown that the targeting of OSBP and CERT to the Golgi is mediated by their PH domains that bind PI4P on the Golgi membranes (Levine and Munro, 2002; Hanada *et al*., 2003). Their impaired targeting to the Golgi of VAP-depleted cells treated with 25OH may therefore result from reduced levels of PI4P in the Golgi complex. To explore this possibility, we assessed the PI4P levels in the Golgi complex using the PH domain of OSBP fused to GFP (GFP-PH-OSBP) as a reporter. As shown in Figure 4A, the Golgi localization of GFP-PH-OSBP was enhanced in control cells treated with 25OH (by ~20%), was slightly reduced in VAP-depleted cells grown in normal media (by ~15%), and was barely detectable in VAP-knockdown cells grown in the presence of 25OH. To further examine the effect of VAPs on the PI4P levels in the Golgi, we characterized the subcellular distribution of γ-adaptin, a subunit of the adaptor complex 1 (AP1) that is recruited to the TGN by PI4P binding (Wang *et al*., 2003). As shown in Figure 4B, γ-adaptin was localized to the Golgi in control cells grown in normal media and in the presence of 25OH. Depletion of VAPs, however, significantly reduced its Golgi association under both growth conditions. These results suggest that knock-down of VAPs directly affects the PI4P levels in the Golgi. The differences in the targeting of GFP-PH-OSBP and γ-adaptin to the Golgi complex of VAP-depleted cells grown under regular growth conditions may result from the different sensitivities of these reporters to PI4P levels or may reflect different PI4P pools.

The impaired targeting of CERT to the Golgi complex of VAP-depleted cells could affect ceramide transport from the ER to the Golgi and the subsequent production of SM by SMS in the lumen of the *trans*-Golgi. This might also affect the level of DAG, because SMS catalyzes the transfer of phosphocholine from PC to ceramide producing SM and DAG (Tafesse *et al*., 2006). We therefore examined the effect of VAP depletion on SM synthesis by applying metabolic labeling with [^{3}H]choline as described in *Materials and Methods*. As shown in Figure 4C, SM production was reduced by ~20% in VAP-depleted cells grown in regular media and by ~40% in VAP-depleted cells grown in the presence of 25OH compared with controls. These results suggest that depletion of VAPs markedly affects SM production, consistent with a previous report (Perry and Ridgway, 2006).

Next, we assessed whether VAP knockdown also affects DAG levels in the Golgi by using the C1b domain of PKCη fused to GFP (GFP-PKCη-C1b) as a reporter. The C1b domain exhibits high affinity for DAG and mediates the targeting of PKCη to the Golgi complex (Maissel *et al*., 2006). As shown in Figure 4D, GFP-PKCη-C1b was localized to the Golgi of control cells grown in normal media and in the presence of 25OH. The latter treatment slightly enhanced its targeting to the Golgi, possibly due to increased DAG production by SMS. Depletion of VAPs, however, reduced the targeting of GFP-PKCη-C1b to the Golgi of cells grown in regular media and apparently abolished its Golgi targeting in response to 25OH. Similar results were obtained using GFP-PKD as a reporter for DAG levels in the TGN (Baron and Malhotra, 2002) (Supplemental Figure S3). Collectively, these results indicate that VAP depletion markedly affects Golgi structure, impairs the Golgi targeting of the FFAT-motif–containing proteins Nir2, OSBP, and CERT and substantially reduces the levels of PI4P, SM, and DAG in the Golgi membranes. All of these effects were more pronounced in the presence of 25OH.

VAP Depletion Causes to Pleiotropic Defects in Golgi-mediated Transport Pathways

We next examined the influence of VAP knockdown on the functional properties of the Golgi complex by applying multiple transport assays. In all assays, we compared transport in control and VAP-depleted cells grown either in normal media or in the presence of 25OH. To assess whether VAP depletion affects ER-to-Golgi or intra-Golgi transport, control and VAPs RNAi-treated HeLa cells were transfected with an expression vector encoding the temperature-sensitive mutant of vesicular stomatitis virus glycoprotein fused to YFP (ts045 YFP-VSV-G), pulse labeled with [^{35}S]methionine at 40°C, and then incubated at 32°C for different times. The sensitivity of VSV-G to endo H digestion was used to monitor VSV-G transport. VSV-G acquires high mannose oligosaccharides in the ER, thereby exhibiting a sensitivity to endo H. However, as it transports through the Golgi apparatus it is modified by *N*-acetyl glucosaminyl transferase and resident mannosidases and becomes resistant to endo H (Balch and Keller, 1986). As shown in Figure 5A, the acquisition of VSV-G endo H resistance was very similar in the control and VAP-depleted cells, suggesting that VAP depletion has no effect on ER-to-Golgi or intra-Golgi transport. We next examined the effect of VAPs on TGN to plasma membrane transport. Control and VAP-depleted cells were infected with ts045 VSV, incubated at 40°C for 3 h, shifted to 20°C for 2.5 h to accumulate VSV-G at the TGN, and finally shifted to 32°C for the indicated times (Figure 5B). Transport was assessed by immunofluorescence analysis and rate of VSV-G export from the TGN was determined by calculating the ratio between TGN-associated VSV-G, which was colocalized with TGN46, to total VSV-G fluorescence. As shown, VAP depletion substantially inhibited VSV-G transport from the TGN to the cell surface. This inhibitory effect was more pronounced in the presence of 25OH (Figure 5B). Live-cell imaging of YFP-VSV-G export from the TGN of VAP-depleted cells suggested that the inhibitory effect of VAP knockdown results from the impaired fission of transport carriers, as

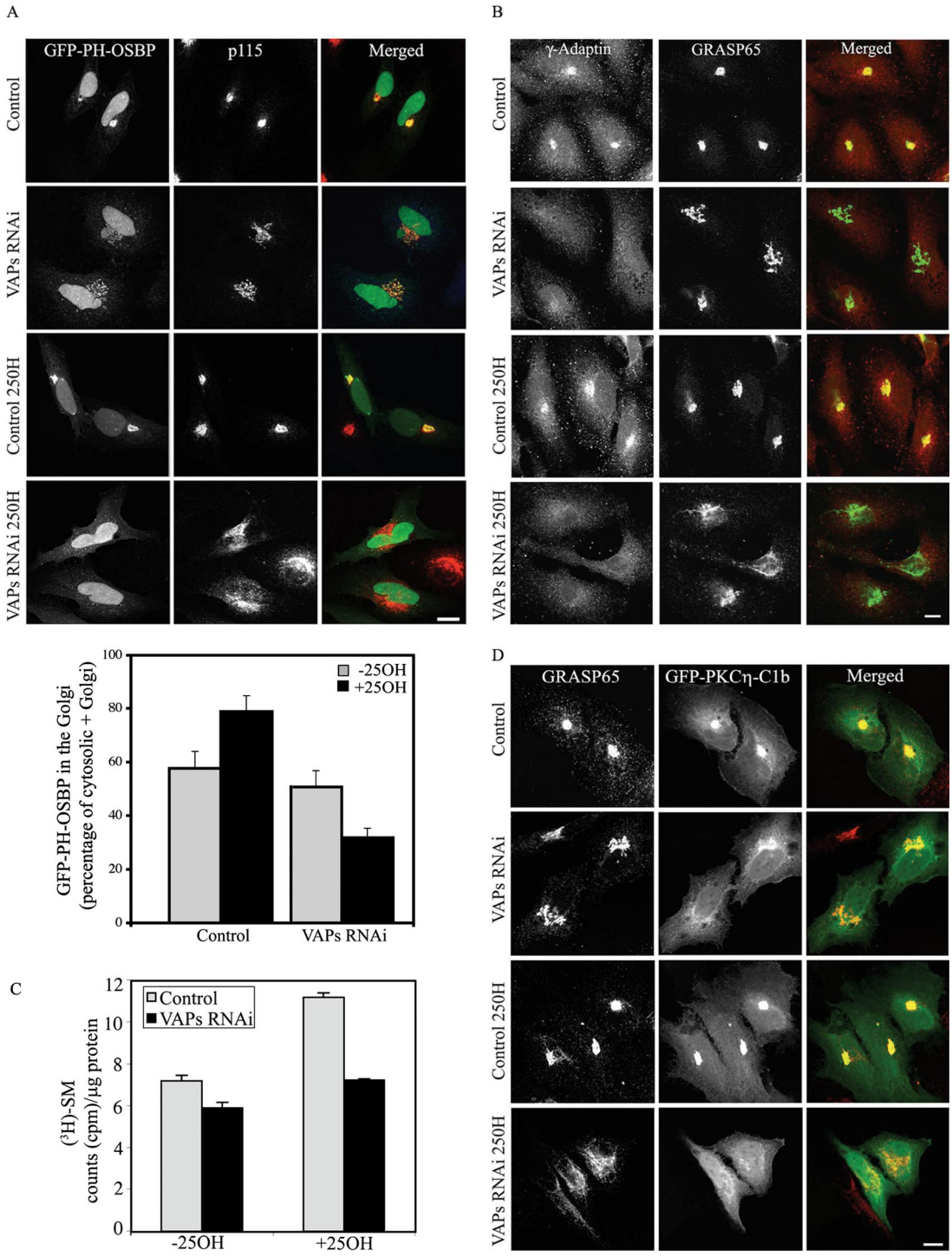

Figure 4. Knockdown of VAPs affects the level of PI4P, SM, and DAG in the Golgi. Control and VAPs RNAi cells were either transfected with GFP-PH-OSBP (A) or left untransfected (B). The cells were treated with 25OH as indicated, fixed, and immunostained with anti p115 (red) (A) or double-immunostained with anti-GRASP65 (green) and anti-γ-adaptin (red) antibodies (B). Representative confocal images are shown. The localization of GFP-PH-OSBP in the Golgi under the described growth conditions was determined by measuring the ratio of Golgi-associated GFP-PH-OSBP (colocalizes with p115) to total GFP-PH-OSBP fluorescence in the Golgi and the cytosol. The data shown are mean values ± SE of two independent experiments, with n = 20 for each condition. Bar, 10 μm. (C) VAPs knockdown affects SM synthesis. Control and VAPs RNAi cells were metabolically labeled with [^{3}H]choline for 12 h in the presence or absence of 25OH. SM production was quantified after TLC separation as described in *Materials and Methods*. The results represent the mean values ± SE of triplicates from three independent experiments. (D) Depletion of VAPs reduces the DAG level in the Golgi. Control and VAPs RNAi cells were transiently transfected with a mammalian expression vector encoding the C1b domain of PKCη fused to GFP (GFP-PKCη-C1b), and 8 h later cells were treated with 25OH for 12 h where indicated. The cells were fixed, immunostained with anti-GRASP65 antibody (red), and analyzed by confocal microscopy. Bar, 10 μm.

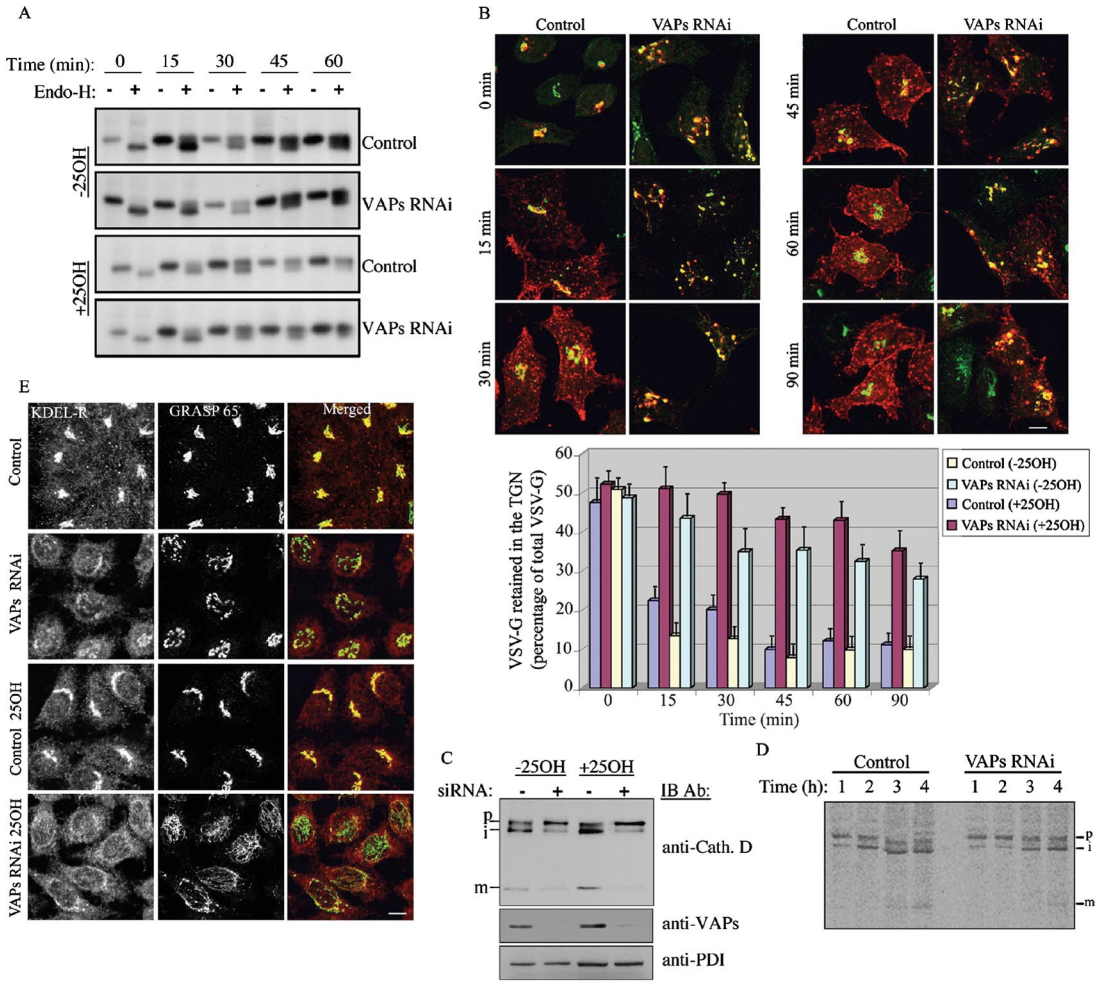

Figure 5. VAPs depletion has a pleiotropic effect on Golgi-mediated transport events. (A) ER-to-Golgi transport is not affected by VAPs RNAi. Control and VAPs RNAi-treated HeLa cells were transiently transfected with an expression vector encoding YFP-VSV-G (ts045). The cells were incubated for 12 h at 40°C in the absence or presence of 25OH, pulse labeled with [^{35}S]methionine for 30 min at 40°C, and chased at 32°C for the indicated times. At each time point, the cells were lysed, VSV-G-YFP was immunoprecipitated with anti-VSV-G antibody, and cells were incubated in the absence or presence of endo H as described in *Materials and Methods*. The samples were analyzed by SDS-PAGE and autoradiography. (B) VAPs depletion inhibits TGN to plasma membrane transport. Control and VAPs RNAi cells were infected with ts045 strain of VSV at 37°C for 30 min, washed, and incubated at 40°C for 3 h. The cells were then shifted to 20°C for 2.5 h to block export from the TGN, and then they were incubated at 32°C for the indicated times, fixed, and double immunostained with anti-VSV-G (red) and anti-TGN46 (green) antibodies. Where indicated, the cells were incubated in the presence of 25OH 6 h before infection and throughout the infection time and temperature shifts. Representative images of 25OH-treated cells at each time point are shown. The rate of VSV-G export from the TGN was determined by measuring the ratio of Golgi-associated VSV-G to total VSV-G fluorescence. The data shown are mean values ± SE of two independent experiments, with n = 50 for each time point in each experiment. Bar, 10 μm. (C) Maturation of cathepsin D is inhibited in VAP-knockdown cells. HeLa cells were transiently transfected with VAPs siRNA, and either treated with 25OH or left untreated. Total cell lysate was prepared and analyzed by Western blotting using anti-cathepsin D antibody. The precursor form of 53-kDa (p), intermediate form of 47-kDa (i), and the mature form of 31-kDa (m) are marked. (D) Pulse-chase metabolic labeling of cathepsin D in 25OH-treated control and VAP-depleted HeLa cells. The cells were metabolically labeled with [^{35}S]methionine-cysteine for 2 h at 20°C and chased for the indicated times at 37°C. Cells were solubilized and the extracts were subjected to immunoprecipitation with anti-Cathepsin D antibody. The immunoprecipitates were analyzed by SDS-PAGE and fluorography. The positions of the p, i, and m heavy chain of Cathepsin D are marked. (E) Distribution of the KDEL receptor in control and VAP-knockdown cells was assessed by indirect immunofluorescence analysis. As shown the KDEL receptor (red) redistributes to the ER in VAP-depleted cells. Bar, 10 μm.

YFP-VSV-G was visualized in multiple long tubules emanating from the TGN (Supplemental Movies M1 and M2). These results are consistent with the role of DAG in the fission of transport carriers at the TGN (Liljedahl *et al.*, 2001; Baron and Malhotra, 2002), and its reduced levels in VAP-knockdown cells. Similarly, the reduced level of PI4P in the TGN of VAP-knockdown cells and the concomitant impaired targeting of γ-adaptin (Figure 4B) could affect clathrin-coated vesicle trafficking between the TGN and the endosome/lysosome system. We therefore examined the effect of VAP knockdown on TGN-to-endosome/lysosome transport by assessing the proteolytic maturation of cathepsin D at steady state. Like many other lysosomal hydrolases, cathepsin D is synthesized in the ER as an inactive (52- to 54-kDa) glycosylated propeptide. It is then tagged with mannose-6-phosphate in the Golgi complex and transported to the endosomes, where it is cleaved into a 47-kDa intermediate form before its final maturation in the lysosomes into a two-chain catalytic enzyme consisting of ~31- and ~15-kDa fragments

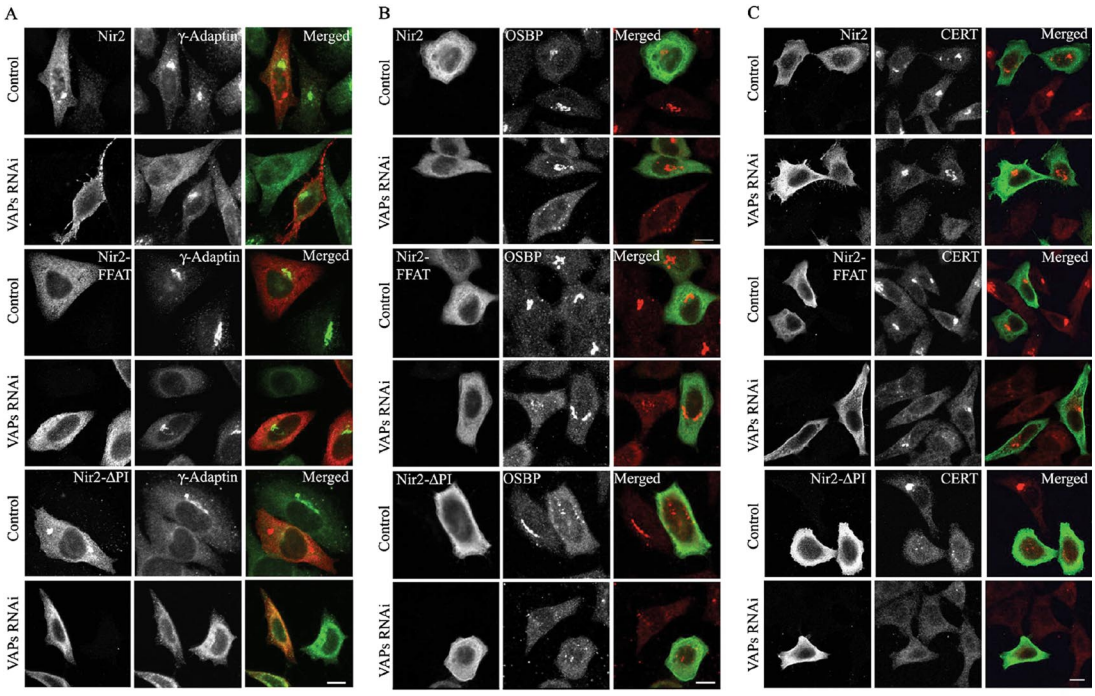

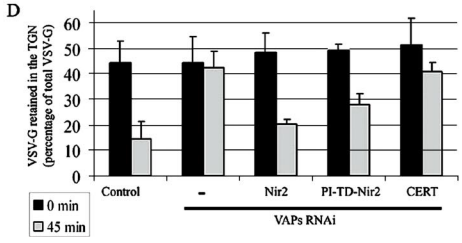

Figure 6. Nir2 restores the PI4P level in the Golgi, the targeting of OSBP and CERT to the Golgi, the Golgi morphology of VAP-depleted cells, and protein transport from the TGN. HeLa cells were transiently transfected with either scrambled (control) or VAPs siRNA duplexes, and 3 d later, the cells were transfected with mammalian expression vectors encoding either the wild-type Nir2-HA, the Nir2-HA FFAT mutant, or the ΔPI mutant. The cells were treated with 25OH for 12 h, fixed, and double immunostained either with anti-HA (red) and anti-γ-adaptin (green) antibodies (A), with anti-HA (green) and anti-OSBP (red) antibodies (B), or anti-HA (green) and anti-CERT (red) antibodies (C). Shown are representative confocal images of VAPs RNAi and control cells. Bar, 10 μm. (D) Nir2 restores VSV-G transport from the TGN to the plasma membrane of 25OH-treated VAP-depleted HeLa cells. VAP-depleted cells were transfected with expression vectors encoding either the wild-type Nir2, the Nir2 PI-transfer domain (PI-TD) (aa 1-277), CERT, or left untransfected (−). Twelve h later the cells were infected with ts045 VSV for 30 min at 37°C, washed, and incubated at 40°C for 3 h. The cells were then shifted to 20°C for 2.5 h to block export from the TGN and then incubated at 32°C for different times, fixed, and double immunostained with anti-VSV-G and anti-TGN46 antibodies. Export of VSV-G from the TGN was determined by measuring the ratio of Golgi-associated VSV-G (colocalizes with TGN46) to total VSV-G fluorescence. The percentage of VSV-G retained at the at time 0 and 45 min after shifting the temperature to 32°C was determined for control cells, or VAP-depleted cells expressing the indicated proteins. The data shown are mean values ± SE of two independent experiments, with n = 30 for each time point in each experiment.

(Mardones *et al.*, 2007). The results shown in Figure 5C clearly demonstrate the inhibitory effect of VAP depletion on cathepsin D maturation, consistent with the effect on γ-adaptin localization (Figure 4B), and the involvement of the AP1 in the sorting of cathepsin D into clathrin-coated vesicles at the TGN (Doray and Kornfeld, 2001). These results were further confirmed by a kinetic analysis of Cathepsin D trafficking using a pulse-chase metabolic labeling experiment. As shown in Figure 5D, depletion of VAPs significantly attenuated Cathepsin D processing, consistent with the steady-state findings. Finally, we examined the effect of VAP depletion on the steady-state distribution of the KDEL-R, a protein that normally cycles between the ER and *cis*-Golgi. As shown, the diffuse ER pattern of KDEL-R markedly increased in VAP-depleted cells treated with 25OH (Figure 5E), suggesting that Golgi-to-ER transport is perturbed in these cells. Collectively, these results indicate that down-regulation of VAPs perturbs protein transport from the Golgi to the endosome/lysosome, to the plasma membrane and to the ER, with no detectable effect on protein transport from the ER to the Golgi.

Nir2 Restores the Level of PI4P in the Golgi, the Golgi Morphology, the Targeting of OSBP and CERT to the Golgi of VAP-Knockdown Cells, and Protein Transport from the TGN

Thus far, we showed that VAP knockdown exerts pleiotropic effects on the Golgi structure and secretory function. We hypothesized that these effects are caused by impaired lipid composition of the Golgi membranes due to mistargeting of CERT, OSBP, and Nir2 in VAP-knockdown cells. Because the Golgi targeting of OSBP and CERT is dependent on the levels of PI4P, which are markedly reduced in VAP-depleted cells (Figure 4, A and B), it could be that elevating the PI4P levels would restore the Golgi targeting of OSBP and CERT, and possibly Golgi structure and function. We showed that VAP knockdown affects the Golgi targeting of Nir2 (Figure 3C), which possesses a PI/PC-transfer activity. This activity might be required for PI transport from the ER to the Golgi. The subsequent phosphorylation of PI to PI4P by Golgi-localized phosphatidylinositol 4-kinases (PI4Ks) could, therefore, produce targeting sites for OSBP and CERT. To explore this possibility, we examined whether Nir2 can re-

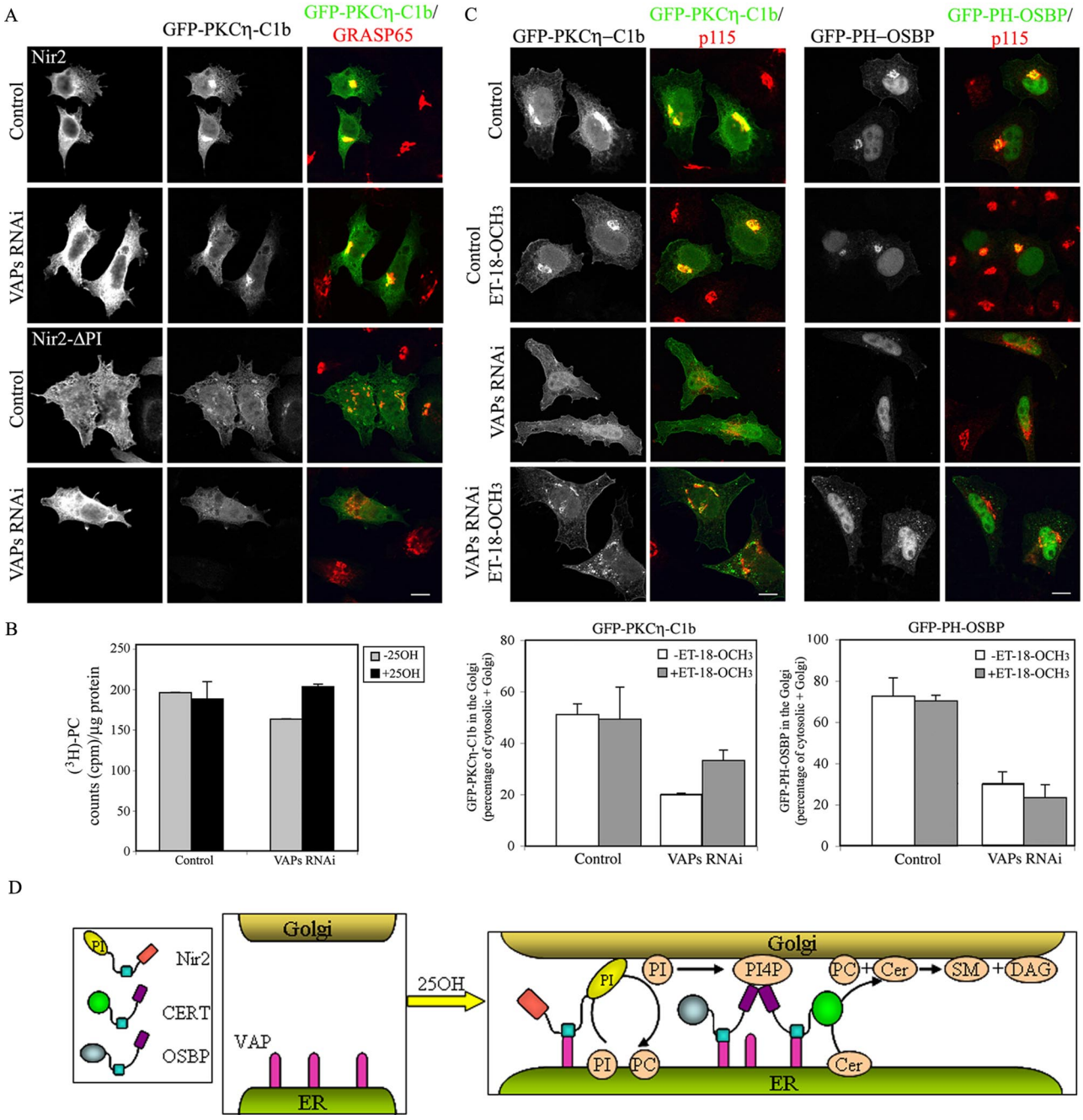

Figure 7. Nir2 restores the DAG level in the Golgi of VAP-depleted cells, and it coordinately functions with OSBP and CERT to control DAG production. (A) HeLa cells were transiently transfected with either scrambled (control) or VAPs siRNA duplexes, and 3 d later were cotransfected with expression vectors encoding the GFP-PKCη-C1b and either the wild-type or the ΔPI mutant of Nir2-HA. Eight hours later the cells were treated for 12 h with 25OH, fixed, double immunostained with anti-HA (white) and anti-GRASP65 (red) antibodies, and analyzed by confocal microscopy using the respective channels for Cy3 (GRASP65), Cy5 (HA), and GFP (GFP-PKCη-C1b). Bar, 10 μm. (B) Knockdown of VAPs affects PC biosynthesis. Control and VAPs RNAi cells were metabolically labeled with [^{3}H]choline for 12 h in the presence or absence of 25OH. PC production was quantified after TLC separation as described in *Materials and Methods*. The results represent the mean values ± SE of triplicates from three independent experiments. (C) Inhibition of the CDP-choline pathway partially restores the DAG levels in the Golgi of VAP-depleted cells without a significant effect on the PI4P levels. Control and VAPs RNAi HeLa cells were transiently transfected with either GFP-PKCη-C1b or GFP-PH-OSBP and 8 h later were treated with 25OH for 12 h. Two hours before fixation, the cells were treated with 10 μM ET-18-OCH$_3$, a nonmetabolizable analogue of lysophosphatidylcholine, which inhibits CCT (Litvak *et al.*, 2005). The cells were then fixed, double immunostained with anti-p115 (red) and anti-VAP (data not shown) antibodies, and analyzed by confocal microscopy. The localization of GFP-PKCη-C1b or GFP-PH-OSBP in the Golgi was determined by measuring the ratio of Golgi-associated GFP-fusion proteins (colocalized with p115) to total GFP fluorescence in the Golgi and the cytosol. The data shown are mean values ± SE of three independent experiments, with n = 30 for each condition. Bar, 10 μm. (D) Model describing the coordinated function of Nir2, OSBP, and CERT at the ER-Golgi membrane contact sites. Nir2, OSBP and CERT contain a FFAT motif (blue) that mediates their interactions with the integral ER-membrane proteins: VAP-A and VAP-B. Treatment with 25OH causes the recruitment of VAPs to the Golgi region (Supplemental Figure S2), possibly the ER–Golgi MCSs, and enhances the targeting of Nir2 to the Golgi membranes (Figure 3C). Nir2 transfers PI or PC via its N-terminal PI-transfer domain (yellow). It transfers PI from the ER to the Golgi,

store the effects of VAP-depletion on Golgi structure and function. First, we reevaluated the level of PI4P in Nir2-knockdown cells by using the GFP-PH-OSBP reporter. Previously, we had found that knockdown of Nir2 has no significant effect on PI4P levels in the Golgi membranes under regular growth conditions (Litvak *et al*., 2005), and reproducible results are shown in Supplemental Figure S4. However, exposure of Nir2-depleted cells to 25OH resulted in cytosolic distribution of GFP-PH-OSBP, suggesting that under these conditions, Nir2 is crucial for PI4P production in the Golgi. Accordingly, we overexpressed either the wild-type Nir2 or Nir2 mutants truncated of the PI-transfer domain (ΔPI) or mutated in the FFAT motif (Amarilio *et al*., 2005) in VAP-depleted cells, and analyzed the subcellular localization of γ-adaptin, OSBP, and CERT in cells grown in the presence of 25OH. The results clearly demonstrate the ability of wild-type Nir2, as well as the FFAT mutant, to restore the targeting of γ-adaptin (Figure 6A), OSBP (Figure 6B), and CERT (Figure 6C) to the Golgi of VAP-depleted cells. Strikingly, they also restored the Golgi morphology of VAP-knockdown cells treated with 25OH (Figure 7A). In contrast, the ΔPI mutant failed to restore the targeting of these proteins, suggesting that the PI-transfer activity of Nir2 is crucial for PI4P production in the Golgi complex under these conditions. Moreover, overexpressing the ΔPI mutant in control cells affected Golgi morphology, PI4P levels, and Golgi targeting of OSBP and CERT in response to 25OH treatment (Figure 6, A–C). These results suggest that this mutant has a dominant negative effect, probably by competing with endogenous Nir2 protein for VAP binding.

It is worth mentioning that the ability of wild-type Nir2 and the FFAT mutant to restore the level of PI4P in the Golgi of VAP-depleted cells was observed when they were highly expressed, consistent with previous results using highly expressed mutants of CERT, which could support ceramide transport from the ER to the Golgi even in the absence of the PH domain or the FFAT motif (Kawano *et al*., 2006). These high expression levels are possibly required for compensating the loss of binding sites on the ER membranes due to VAPs knockdown.

Next, we examined whether Nir2 can also restore protein transport from the TGN to the PM of 25OH-treated VAP-depleted cells applying the VSV-G transport assay described in Figure 5B. In this set of experiments, we expressed either the wild-type Nir2, its PI-transfer domain (aa 1–277), or CERT in VAP-knockdown cells. The cells were infected with ts045 VSV, and VSV-G transport from the TGN to the PM was analyzed after shifting the temperature from a 20°C block to 32°C. The results clearly show that wild-type Nir2 had the most profound effect (Figure 6D). It almost completely restored the transport defect of VAP-depleted cells. In contrast, the PI-transfer domain had only a partial effect, whereas CERT had a minor effect. The partial effect of the PI-transfer domain on VSV-G transport is consistent with its inability to fully restore the Golgi morphology and Golgi targeting of OSBP and CERT in VAP-knockdown cells (Supplemental Figure S5). Collectively, these results suggest that the PI-transfer domain is crucial for Nir2 function; yet, it is insufficient when expressed as an isolated domain. These results are consistent with our previous findings demonstrating that the PI-transfer domain failed to fully restore the phenotype of Nir2-depleted cells (Litvak *et al*., 2005).

Nir2 Restores DAG Levels in the Golgi of VAP-depleted Cells and Regulates DAG Production and Consumption

Next, we examined whether Nir2 can also restore DAG levels in the Golgi of VAP-depleted cells by applying the experimental strategy described for PI4P, using the GFP-PKCη-C1b reporter. As shown in Figure 7A, the ability of Nir2 to restore DAG levels in the Golgi of VAP-depleted cells was dependent on its PI-transfer domain. Thus, Nir2 could restore both PI4P and DAG levels in the Golgi of VAP-depleted cells. Because Nir2 is a PI/PC-transfer protein, it could be that its PI-transfer activity is required for PI4P production, OSBP and CERT targeting, and the subsequent production of SM and DAG. Its PC-transfer activity, in contrast, may regulate DAG consumption via the CDP-choline pathway for PC biosynthesis (Lev, 2006). We have previously shown that Nir2 negatively regulates the CDP-choline pathway and thereby affects DAG levels in the Golgi (Litvak *et al*., 2005). We therefore examined whether the CDP-choline pathway is also involved in regulating the level of DAG in the Golgi of VAP-depleted cells. Two experimental approaches were applied: measuring PC synthesis after metabolic labeling with [^{3}H]choline as described in *Materials and Methods*, and assessing the level of DAG in the Golgi of VAP-depleted cells, by using the GFP-PKCη-C1b reporter, after inhibition of the CDP-choline pathway. As shown in Figure 7B, 25OH had no effect on PC biosynthesis in the control cells (the ratio between treated and untreated cells was very close to 1), but it enhanced PC biosynthesis in VAP-depleted cells (the ratio was ~1.22), suggesting that under these conditions, DAG consumption is accelerated. Furthermore, inhibition of the CDP-choline pathway by the CTP:phosphocholine cytidylyltransferase (CCT) inhibitor ET-18-OCH_3 (Litvak *et al*., 2005), only partially restored the DAG levels and morphology of the Golgi in VAP-depleted cells treated with 25OH, but it had no detectable effect on the PI4P levels (Figure 7C). Likewise, ET-18-OCH_3 partially restored the DAG level in the Golgi of Nir2-RNAi cells grown in the presence of 25OH, but it fully restored it in cells grown in normal media (Supplemental Figure S6). These results suggest that both production and consumption of DAG are affected by VAP-knockdown. Accordingly, we propose that VAPs are critical for Nir2 targeting to the Golgi in response to 25OH (Figure 3C) and that Nir2, via its dual lipid-transfer activity, can regulate both the production and consumption of DAG at the ER–Golgi MCSs, as illustrated in Figure 7D.

DISCUSSION

In this study, we show that the integral ER–membrane proteins VAP-A and VAP-B are required for maintaining the structural and functional properties of the Golgi complex (Figures 2 and 5) by regulating the levels of key lipids in the Golgi membranes. Knockdown of VAPs substantially reduces the levels of PI4P, DAG, and SM in the Golgi membranes (Figure 4) and concomitantly exerts pleiotropic effects on Golgi-mediated transport events (Figure 5). These

down the PI concentration gradient, and PC back from the Golgi to the ER. This direction of lipid exchange between the ER and the Golgi is critical for regulation of the subsequent events: PI in the Golgi is phosphorylated by Golgi-localized PI4Ks, producing PI4P, which recruits OSBP and CERT by direct binding of their PH domains (purple). CERT then transfers ceramide (Cer) from the ER to the Golgi, which enables the production of SM and DAG in the *trans*-Golgi. Concomitantly, the transfer of PC from the Golgi to the ER probably inhibits the CDP-choline pathway for PC biosynthesis, thereby regulating DAG consumption.

observations are consistent with the established roles of these lipids in the regulation of membrane trafficking (Huijbregts *et al.*, 2000; van Meer and Sprong, 2004). DAG, a strongly conical lipid that induces negative membrane curvature, is essential for fission of transport carriers at the TGN (Liljedahl *et al.*, 2001; Baron and Malhotra, 2002; Corda *et al.*, 2002). Indeed, protein transport from the TGN to the plasma membrane was markedly attenuated in VAP-knockdown cells (Figure 5B), and impaired fission of transport carriers was demonstrated by real-time imaging of YFP-VSV-G export from the TGN (Supplemental Movie M2). PI4P is required for recruitment of clathrin adaptor AP1 to the TGN (Wang *et al.*, 2003), thereby regulating clathrin-coated vesicle trafficking between the TGN and endosome/lysosme system (Doray and Kornfeld, 2001; Mills *et al.*, 2003). Its reduced levels in the Golgi of VAP-depleted cells are consistent with the inhibitory effect of VAP knockdown on Cathepsin D maturation (Figure 5, C and D). Although PI4P does not seem to have a direct role in TGN to plasma membrane transport, current studies suggest that PKD, which is recruited and activated by DAG at the TGN, phosphorylates PI4KIIIβ, and stimulates its lipid-kinase activity, and that PKD-mediated phosphorylation of PI4KIIIβ enhances VSV-G transport to the plasma membrane (Hausser *et al.*, 2005). DAG was also implicated in the regulation of Golgi-to-ER retrograde transport (Fernandez-Ulibarri *et al.*, 2007), which might explain the impaired steady-state distribution of KDEL-R in VAP-knockdown cells (Figure 5E).

We further showed that VAPs are required for Golgi targeting of Nir2, OSBP, and CERT in response to 25OH treatment (Figure 3, A–C), suggesting that lipid transfer by these LT/BPs is spatially restricted to ER–Golgi MCSs under these particular conditions. This hypothesis is supported by the redistribution of VAPs to the perinuclear region (Supplemental Figure S2), by the enhanced interaction of VAPs with Nir2, OSBP, and CERT (Figure 3D), and the enhanced Golgi-targeting of these FFAT proteins (Figure 3, A–C) in response to 25OH treatment. Furthermore, previous studies suggest that 25OH enhances CERT-mediated ceramide transport (Perry and Ridgway, 2006) and that mutations within its FFAT motif impair ER-to-Golgi ceramide transport (Kawano *et al.*, 2006). These findings are consistent with the reduced SM synthesis in VAP-knockdown cells (Figure 4C). Collectively, these results suggest that VAP-depletion affects the Golgi-targeting of Nir2, OSBP, and CERT, thereby impairing nonvesicular lipid transfer at the ER–Golgi MCSs, and consequently affecting the lipid composition of the Golgi membranes and their structural and functional properties. This hypothesis is further supported by the ability of the PI/PC-transfer protein, Nir2, to restore the levels of PI4P (Figure 6) and DAG (Figure 7A) in the Golgi of VAP-knockdown cells treated with 25OH, as well as the Golgi morphology (Figure 7A), in a PI/PC-transfer activity–dependent manner. The PI/PC-transfer domain of Nir2 was also required for restoring the Golgi-targeting of OSBP and CERT in VAP-knockdown cells (Figure 6, B and C). These observations demonstrate the crucial role of the PI/PC-transfer activity of Nir2. Yet, an isolated PI-transfer domain of Nir2 failed to fully restore either the Golgi targeting of OSBP or CERT (Supplemental Figure S5), or protein transport from the TGN to the PM (Figure 6D), suggesting that although the PI-transfer domain is necessary, it is insufficient for fully restoring Nir2 functions. These observations are inconsistent with previous studies on the *Drosophila* homologue rdgB, which proposed that the complete repertoire of rdgB functions resides in its PI-transfer domain (Milligan *et al.*, 1997).

Although Nir2 and rdgB are functionally interchangeable in *Drosophila* photoreceptor cells (Chang *et al.*, 1997), the inconsistency with our results could be cell type specific. Early localization studies of rdgB in photoreceptor cells suggest that it is localized to the subrhabdomeric cisternal (SRC) membranes adjacent to the rhabdomeres (Vihtelic *et al.*, 1993; Suzuki and Hirosawa, 1994). The SRC is an extensive network of membranes derived from the rough ER and thought to play a critical role in maintenance of the rhabdomeric membranes (Matsumoto-Suzuki *et al.*, 1989). This localization of rdgB in the SRC adjacent to plasma membrane at the bases of photoreceptive microvilli may represent ER-PM MCSs (Suzuki and Hirosawa, 1994). Thus, rdgB and its homologues, such as Nir2, can be localized to different MCSs in a cell–type-specific manner. Furthermore, it was proposed that rdgB is required for transport of PI from the SRC into the rhabdomeric microvilli, where it is phosphorylated to phosphatidylinositol bisphosphate (PIP_2). In *rdgB* mutants, light activation of phospholipase C hydrolyzes PIP_2. Because PI cannot be replenished in the rhabdomeres of *rdgB* mutants, the membrane experiences a decrease in PI or PIP_2 levels, thereby leading to degeneration (Vihtelic *et al.*, 1993). Consistent with this hypothesis, we show here that Nir2 can restore the Golgi morphology of VAP-depleted cells in its PI-transfer activity-dependent manner. Thus, both Nir2 and rdgB probably transfer PI at MCSs, but in the cellular system used in this study, Nir2 functions at the ER–Golgi rather than the ER–PM MCSs.

Accordingly, we propose that Nir2 transfers PI from the ER to the Golgi, down the PI concentration gradient. PI is then phosphorylated by Golgi-localized PI4Ks, producing PI4P, which recruits OSBP and CERT by binding to their PH domains. This enables ER-to-Golgi ceramide transport and the subsequent production of DAG and SM (Figure 7D). Because Nir2 is a PI/PC-exchange protein that transfers PI from a donor membrane and removes PC from an acceptor membrane, its ER-to-Golgi PI-transfer activity must be coupled to its Golgi-to-ER PC-transfer activity. Transport of PC from the Golgi to the ER may inhibit CCT activity, thereby regulating the CDP-choline pathway for PC biosynthesis, which consumes DAG (Lev, 2006). Our previous studies suggest that Nir2 negatively regulates this pathway, because its down-regulation reduced DAG levels in the Golgi and enhanced PC biosynthesis. Inhibition of the CDP-choline pathway, however, restored the DAG level in the Golgi of Nir2-RNAi cells (Litvak *et al.*, 2005). Here, we found that PC biosynthesis was slightly increased in VAP-knockdown cells treated with 25OH compared with control and that a CCT inhibitor partially restored the DAG level in their Golgi membranes (Figure 7, B and C). This suggests that mistargeting of Nir2 in VAP-knockdown cells affects both DAG production by SMS and DAG consumption via the CDP–choline pathway. According to the proposed model shown in Figure 7D, the transfer of PI from the ER to the Golgi and PC back, would facilitate an increase in the Golgi DAG levels. However, this increase must be negatively regulated to maintain a critical pool of DAG in this organelle. Indeed, current studies have shown that PKD phosphorylates CERT and that this phosphorylation decreases its affinity for the Golgi membranes thereby reducing ceramide transfer from the ER to the Golgi (Fugmann *et al.*, 2007). This could be a potential mechanism for regulating the production of DAG by SMS. Phosphorylation of Nir2 at its PI-transfer domain by DAG-activated Golgi localized PKCs, could also provide a mechanism for negatively regulating DAG levels in the Golgi. Previous studies on PI-transfer proteins have shown that phosphorylation of highly conserved residues affects

their PI/PC-exchange activity (van Tiel *et al*., 2000; Morgan *et al*., 2004). Thus, it could be that similar phosphorylation in the PI-transfer domain of Nir2 affects its PI- and/or-PC-transfer activity, thereby inhibiting DAG production and/or accelerating its consumption.

Overall, our results suggest that Nir2, OSBP, and CERT function coordinately at the ER-Golgi MCSs. CERT and Nir2 are likely to be involved in lipid transport, because they transfer lipids between membrane bilayers in vitro (Fullwood *et al*., 1999; Kumagai *et al*., 2005). OSBP, in contrast, might not be directly involved in lipid transport but rather in lipid sensing. Its ability to bind oxysterols and stimulate SM synthesis (Ridgway, 1995), suggest a potential role in the interface between cholesterol and sphingolipid metabolism (Ridgway, 2000). Indeed, current studies proposed that OSBP is involved in sensing and integrating changes in cellular sterol levels with synthesis of SM at the Golgi apparatus by regulating CERT-dependent ceramide transport (Perry and Ridgway, 2006). In this study, we show that Nir2-mediated phospholipid transport coordinately functions with OSBP and CERT, providing new insight into the mechanism that coregulates phospholipid, sphingolipid, and cholesterol metabolism (Ridgway *et al*., 1999).

In summary, our results show that the coordinated function of Nir2, OSBP, and CERT, at the ER–Golgi MCSs requires the VAP proteins, and it is critical for maintaining the structural and functional identity of the Golgi complex. We propose that this coordination integrates interconnected metabolic pathways to tightly control the lipid composition of the Golgi membranes.

ACKNOWLEDGMENTS

Sima Lev is incumbent of the Joyce and Ben B. Eisenberg chair of molecular biology and cancer research. This work was supported by the Minerva foundation with funding from the Federal German Ministry for education and research and by the Israel Science Foundation Grant No. 548/08.

REFERENCES

Amarilio, R., Ramachandran, S., Sabanay, H., and Lev, S. (2005). Differential regulation of endoplasmic reticulum structure through VAP-Nir protein interaction. J. Biol. Chem. *280*, 5934–5944.

Balch, W. E., and Keller, D. S. (1986). ATP-coupled transport of vesicular stomatitis virus G protein. Functional boundaries of secretory compartments. J. Biol. Chem. *261*, 14690–14696.

Baron, C. L., and Malhotra, V. (2002). Role of diacylglycerol in PKD recruitment to the TGN and protein transport to the plasma membrane. Science *295*, 325–328.

Chang, J. T., Milligan, S., Li, Y., Chew, C. E., Wiggs, J., Copeland, N. G., Jenkins, N. A., Campochiaro, P. A., Hyde, D. R., and Zack, D. J. (1997). Mammalian homolog of *Drosophila* retinal degeneration B rescues the mutant fly phenotype. J. Neurosci. *17*, 5881–5890.

Corda, D., Hidalgo Carcedo, C., Bonazzi, M., Luini, A., and Spano, S. (2002). Molecular aspects of membrane fission in the secretory pathway. Cell Mol. Life Sci. *59*, 1819–1832.

De Matteis, M. A., Di Campli, A., and D'Angelo, G. (2007). Lipid-transfer proteins in membrane trafficking at the Golgi complex. Biochim. Biophys. Acta *1771*, 761–768.

Doray, B., and Kornfeld, S. (2001). Gamma subunit of the AP-1 adaptor complex binds clathrin: implications for cooperative binding in coated vesicle assembly. Mol. Biol. Cell *12*, 1925–1935.

Fernandez-Ulibarri, I., Vilella, M., Lazaro-Dieguez, F., Sarri, E., Martinez, S. E., Jimenez, N., Claro, E., Merida, I., Burger, K. N., and Egea, G. (2007). Diacylglycerol is required for the formation of COPI vesicles in the Golgi-to-ER transport pathway. Mol. Biol. Cell *18*, 3250–3263.

Fugmann, T., Hausser, A., Schoffler, P., Schmid, S., Pfizenmaier, K., and Olayioye, M. A. (2007). Regulation of secretory transport by protein kinase D-mediated phosphorylation of the ceramide transfer protein. J. Cell Biol. *178*, 15–22.

Fullwood, Y., dos Santos, M., and Hsuan, J. J. (1999). Cloning and characterization of a novel human phosphatidylinositol transfer protein, rdgBbeta. J. Biol. Chem. *274*, 31553–31558.

Funato, K., and Riezman, H. (2001). Vesicular and nonvesicular transport of ceramide from ER to the Golgi apparatus in yeast. J. Cell Biol. *155*, 949–959.

Hanada, K. (2006). Discovery of the molecular machinery CERT for endoplasmic reticulum-to-Golgi trafficking of ceramide. Mol. Cell Biochem. *286*, 23–31.

Hanada, K., Kumagai, K., Tomishige, N., and Kawano, M. (2007). CERT and intracellular trafficking of ceramide. Biochim. Biophys. Acta *1771*, 644–653.

Hanada, K., Kumagai, K., Yasuda, S., Miura, Y., Kawano, M., Fukasawa, M., and Nishijima, M. (2003). Molecular machinery for non-vesicular trafficking of ceramide. Nature *426*, 803–809.

Hausser, A., Storz, P., Martens, S., Link, G., Toker, A., and Pfizenmaier, K. (2005). Protein kinase D regulates vesicular transport by phosphorylating and activating phosphatidylinositol-4 kinase IIIbeta at the Golgi complex. Nat. Cell Biol. *7*, 880–886.

Holthuis, J. C., and Levine, T. P. (2005). Lipid traffic: floppy drives and a superhighway. Nat. Rev. Mol. Cell Biol. *6*, 209–220.

Huijbregts, R. P., Topalof, L., and Bankaitis, V. A. (2000). Lipid metabolism and regulation of membrane trafficking. Traffic *1*, 195–202.

Kaiser, S. E., Brickner, J. H., Reilein, A. R., Fenn, T. D., Walter, P., and Brunger, A. T. (2005). Structural basis of FFAT motif-mediated ER targeting. Structure *13*, 1035–1045.

Kawano, M., Kumagai, K., Nishijima, M., and Hanada, K. (2006). Efficient trafficking of ceramide from the endoplasmic reticulum to the Golgi apparatus requires a VAMP-associated protein-interacting FFAT motif of CERT. J. Biol. Chem. *281*, 30279–30288.

Kumagai, K., Yasuda, S., Okemoto, K., Nishijima, M., Kobayashi, S., and Hanada, K. (2005). CERT mediates intermembrane transfer of various molecular species of ceramides. J. Biol. Chem. *280*, 6488–6495.

Ladinsky, M. S., Mastronarde, D. N., McIntosh, J. R., Howell, K. E., and Staehelin, L. A. (1999). Golgi structure in three dimensions: functional insights from the normal rat kidney cell. J. Cell Biol. *144*, 1135–1149.

Lagace, T. A., Byers, D. M., Cook, H. W., and Ridgway, N. D. (1999). Chinese hamster ovary cells overexpressing the oxysterol binding protein (OSBP) display enhanced synthesis of sphingomyelin in response to 25-hydroxycholesterol. J. Lipid Res. *40*, 109–116.

Lev, S. (2006). Lipid homoeostasis and Golgi secretory function. Biochem. Soc. Trans. *34*, 363–366.

Lev, S., Ben Halevy, D., Peretti, D., and Dahan, N. (2008). The VAP protein family: from cellular functions to motor neuron disease. Trends Cell Biol. *18*, 282–290.

Levine, T. (2004). Short-range intracellular trafficking of small molecules across endoplasmic reticulum junctions. Trends Cell Biol. *14*, 483–490.

Levine, T., and Loewen, C. (2006). Inter-organelle membrane contact sites: through a glass, darkly. Curr. Opin. Cell Biol. *18*, 371–378.

Levine, T. P., and Munro, S. (2002). Targeting of Golgi-specific pleckstrin homology domains involves both PtdIns 4-kinase-dependent and -independent components. Curr. Biol. *12*, 695–704.

Liljedahl, M., Maeda, Y., Colanzi, A., Ayala, I., Van Lint, J., and Malhotra, V. (2001). Protein kinase D regulates the fission of cell surface destined transport carriers from the trans-Golgi network. Cell *104*, 409–420.

Litvak, V., Dahan, N., Ramachandran, S., Sabanay, H., and Lev, S. (2005). Maintenance of the diacylglycerol level in the Golgi apparatus by the Nir2 protein is critical for Golgi secretory function. Nat. Cell Biol. *7*, 225–234.

Litvak, V., Shaul, Y. D., Shulewitz, M., Amarilio, R., Carmon, S., and Lev, S. (2002). Targeting of Nir2 to lipid droplets is regulated by a specific threonine residue within its PI-transfer domain. Curr. Biol. *12*, 1513–1518.

Loewen, C. J., Roy, A., and Levine, T. P. (2003). A conserved ER targeting motif in three families of lipid binding proteins and in Opi1p binds VAP. EMBO J. *22*, 2025–2035.

Maissel, A., Marom, M., Shtutman, M., Shahaf, G., and Livneh, E. (2006). PKCeta is localized in the Golgi, ER and nuclear envelope and translocates to the nuclear envelope upon PMA activation and serum-starvation: C1b domain and the pseudosubstrate containing fragment target PKCeta to the Golgi and the nuclear envelope. Cell Signal. *18*, 1127–1139.

Mardones, G. A., Burgos, P. V., Brooks, D. A., Parkinson-Lawrence, E., Mattera, R., and Bonifacino, J. S. (2007). The trans-Golgi network accessory protein p56 promotes long-range movement of GGA/clathrin-containing transport carriers and lysosomal enzyme sorting. Mol. Biol. Cell *18*, 3486–3501.

Marsh, B. J., Mastronarde, D. N., Buttle, K. F., Howell, K. E., and McIntosh, J. R. (2001). Organellar relationships in the Golgi region of the pancreatic beta cell line, HIT-T15, visualized by high resolution electron tomography. Proc. Natl. Acad. Sci. USA *98*, 2399–2406.

Marsh, B. J., Volkmann, N., McIntosh, J. R., and Howell, K. E. (2004). Direct continuities between cisternae at different levels of the Golgi complex in glucose-stimulated mouse islet beta cells. Proc. Natl. Acad. Sci. USA *101*, 5565–5570.

Matsumoto-Suzuki, E., Hirosawa, K., and Hotta, Y. (1989). Structure of the subrhabdomeric cisternae in the photoreceptor cells of *Drosophila melanogaster*. J. Neurocytol. *18*, 87–93.

Milligan, S. C., Alb, J. G., Jr., Elagina, R. B., Bankaitis, V. A., and Hyde, D. R. (1997). The phosphatidylinositol transfer protein domain of *Drosophila* retinal degeneration B protein is essential for photoreceptor cell survival and recovery from light stimulation. J. Cell Biol. *139*, 351–363.

Mills, I. G., Praefcke, G. J., Vallis, Y., Peter, B. J., Olesen, L. E., Gallop, J. L., Butler, P. J., Evans, P. R., and McMahon, H. T. (2003). EpsinR: an AP1/clathrin interacting protein involved in vesicle trafficking. J. Cell Biol. *160*, 213–222.

Mogelsvang, S., Marsh, B. J., Ladinsky, M. S., and Howell, K. E. (2004). Predicting function from structure: 3D structure studies of the mammalian Golgi complex. Traffic *5*, 338–345.

Morgan, C. P. *et al*. (2004). Phosphorylation of a distinct structural form of phosphatidylinositol transfer protein alpha at Ser166 by protein kinase C disrupts receptor-mediated phospholipase C signaling by inhibiting delivery of phosphatidylinositol to membranes. J. Biol. Chem. *279*, 47159–47171.

Perkins, G., Renken, C., Martone, M. E., Young, S. J., Ellisman, M., and Frey, T. (1997). Electron tomography of neuronal mitochondria: three-dimensional structure and organization of cristae and membrane contacts. J. Struct. Biol. *119*, 260–272.

Perry, R. J., and Ridgway, N. D. (2006). Oxysterol-binding protein and vesicle-associated membrane protein-associated protein are required for sterol-dependent activation of the ceramide transport protein. Mol. Biol. Cell *17*, 2604–2616.

Pomorski, T., Hrafnsdottir, S., Devaux, P. F., and van Meer, G. (2001). Lipid distribution and transport across cellular membranes. Semin. Cell Dev. Biol. *12*, 139–148.

Ridgway, N. D. (1995). 25-Hydroxycholesterol stimulates sphingomyelin synthesis in Chinese hamster ovary cells. J. Lipid Res. *36*, 1345–1358.

Ridgway, N. D. (2000). Interactions between metabolism and intracellular distribution of cholesterol and sphingomyelin. Biochim. Biophys. Acta *1484*, 129–141.

Ridgway, N. D., Byers, D. M., Cook, H. W., and Storey, M. K. (1999). Integration of phospholipid and sterol metabolism in mammalian cells. Prog. Lipid Res. *38*, 337–360.

Shore, G. C., and Tata, J. R. (1977). Two fractions of rough endoplasmic reticulum from rat liver. I. Recovery of rapidly sedimenting endoplasmic reticulum in association with mitochondria. J. Cell Biol. *72*, 714–725.

Sprong, H., van der Sluijs, P., and van Meer, G. (2001). How proteins move lipids and lipids move proteins. Nat. Rev. Mol. Cell Biol. *2*, 504–513.

Storey, M. K., Byers, D. M., Cook, H. W., and Ridgway, N. D. (1998). Cholesterol regulates oxysterol binding protein (OSBP) phosphorylation and Golgi localization in Chinese hamster ovary cells: correlation with stimulation of sphingomyelin synthesis by 25-hydroxycholesterol. Biochem. J. *336*, 247–256.

Suzuki, E., and Hirosawa, K. (1994). Immunolocalization of a Drosophila phosphatidylinositol transfer protein (rdgB) in normal and rdgA mutant photoreceptor cells with special reference to the subrhabdomeric cisternae. J. Electron Microsc. *43*, 183–189.

Tafesse, F. G., Ternes, P., and Holthuis, J. C. (2006). The multigenic sphingomyelin synthase family. J. Biol. Chem. *281*, 29421–29425.

van Meer, G. (1993). Transport and sorting of membrane lipids. Curr. Opin. Cell Biol. *5*, 661–673.

van Meer, G. (2000). Cellular organelles: how lipids get there, and back. Trends Cell Biol. *10*, 550–552.

van Meer, G., and Sprong, H. (2004). Membrane lipids and vesicular traffic. Curr. Opin. Cell Biol. *16*, 373–378.

van Tiel, C. M., Westerman, J., Paasman, M., Wirtz, K. W., and Snoek, G. T. (2000). The protein kinase C-dependent phosphorylation of serine 166 is controlled by the phospholipid species bound to the phosphatidylinositol transfer protein alpha. J. Biol. Chem. *275*, 21532–21538.

Vihtelic, T. S., Goebl, M., Milligan, S., O'Tousa, J. E., and Hyde, D. R. (1993). Localization of *Drosophila* retinal degeneration B, a membrane-associated phosphatidylinositol transfer protein. J. Cell Biol. *122*, 1013–1022.

Wang, Y. J., Wang, J., Sun, H. Q., Martinez, M., Sun, Y. X., Macia, E., Kirchhausen, T., Albanesi, J. P., Roth, M. G., and Yin, H. L. (2003). Phosphatidylinositol 4 phosphate regulates targeting of clathrin adaptor AP-1 complexes to the Golgi. Cell *114*, 299–310.

Wyles, J. P., McMaster, C. R., and Ridgway, N. D. (2002). Vesicle-associated membrane protein-associated protein-A (VAP-A) interacts with the oxysterol-binding protein to modify export from the endoplasmic reticulum. J. Biol. Chem. *277*, 29908–29918.